XII International Conference on Computational Plasticity. Fundamentals and Applications
COMPLAS XII
E. Oñate, D.R.J. Owen, D. Peric and B. Suárez (Eds)

CRYSTAL PLASTICITY MODEL CALIBRATION FOR 316L STAINLESS STEEL SINGLE CRYSTALS DURING DEFORMATION

SAMIR EL SHAWISH*, MATEJ BOGATAJ* AND LEON CIZELJ*

*Reactor Engineering Division
Jožef Stefan Institute
Jamova cesta 39, SI-1000 Ljubljana, Slovenia
e-mails: Samir.ElShawish@ijs.si, Bogataj.Bogataj@gmail.com, Leon.Cizelj@ijs.si
web pages: http://r4.ijs.si/elshawish-e, http://r4.ijs.si/cizelj-e

Key words: Slip-based Crystal Plasticity Finite Element Model, Type 316L Stainless Steel Single Crystals

Abstract.

Type 316L austenitic stainless steel is an important structural material used for the in-core components and pressure boundaries of light water reactors. In order to study degradation mechanisms in such a steel, like crack initiation and propagation, it is crucial to develop reliable crystal plasticity models at microscale that would account for anisotropic nature of the material and realistic modelling of grain topology. In this work we present a procedure for calibrating material properties of a slip-based crystal plasticity finite element model and investigate its suitability as a constitutive model for single-crystal tensile test simulations. The material properties include the anisotropic elastic and crystal plasticity material parameters that are calibrated against experimental tensile test curves for 316L stainless steel single crystals at selected crystallographic orientations. For the crystal plasticity material parameters a systematic sensitivity study using Bassani and Wu hardening law is performed.

1 INTRODUCTION

Type 316L austenitic stainless steel is a common structural material in nuclear power reactors. It undergoes degradation due to severe operational conditions (high irradiation, stresses and corrosive environment) that may limit its operational life. To understand the material behavior of these steels under such conditions, modelling of material properties at increasingly smaller scales is becoming more and more important. Efforts are being made to incorporate random grain structure, texture and increasingly sophisticated material models [1] that on the grain-size level often are based on the crystal plasticity theory.

Determination of material parameters for crystal plasticity models is obviously of immense importance. In an ideal case, the parameters can be obtained from tensile test experiments on manufactured single crystal specimens with different crystallographic orientations. However, it is not always possible to manufacture single crystals, which at the end limits the material model calibration to using only macroscopic, polycrystalline response [2, 3]. In the case of 316L stainless steel, it is extremely challenging to grow single crystals, which is why only few reports on single crystal studies exist in literature [4, 5].

In Ref. [4] tensile experiments on single-crystal 316L stainless steel (with a composition of 17% Cr, 12% Ni, 2% Mn, and 0.75% Si) demonstrated a strong orientation dependence on stages of deformation and governing deformation mechanisms. A unique observation was the occurrence of twinning at low strains in all investigated tensile directions: [001], [111] and [123]. The challenge in modelling and predicting the stress-strain response and texture evolution in this type of steel was the consideration of several microstructural mechanisms (twinning, slip, interstitial content, and precipitation hardening) at the same time, length scales associated with them, and interactions between mechanisms. For this purpose, a viscoplastic self-consistent crystal plasticity model was developed and used to simulate the stress-strain response of 316L stainless steel single crystals [4].

In this paper a calibration of material parameters for crystal plasticity finite element model of type 316L stainless steel is performed. The calibration is provided against measured true stress versus true inelastic strain responses of 316L stainless steel single crystals strained along [001], [111] and [123] directions [4]. In a crystal plasticity model only slip is considered as the governing mechanism for plastic deformation.

The structure of the paper is as follows. First, a model description is given with outlining the employed slip-based crystal plasticity constitutive theory and finite element model. Second, a description of the calibration procedure for crystal plasticity material parameters is explained. Finally, the results are presented and conclusions are given at the end.

2 MODEL DESCRIPTION

2.1 Constitutive model

A single crystal is assumed to behave as an anisotropic continuum. Constitutive relations in linear elasticity are given by the generalized Hooke's law:

$$\sigma_{ij} = C_{ijkl}\epsilon_{kl} \tag{1}$$

where σ_{ij} represents the second rank stress tensor, C_{ijkl} the fourth rank stiffness tensor and ϵ_{ij} the second rank strain tensor. Indices i, j, k and l are running from 1 to 3. A cubic crystal lattice symmetry imposes three independent constants $c_{11}(= C_{1111})$, $c_{12}(= C_{1122})$ and $c_{14}(= C_{1212})$ that are taken here from literature for 316L stainless steel [6]: $c_{11} = 204600$ MPa, $c_{12} = 137700$ MPa, $c_{14} = 126200$ MPa.

The plastic behavior of the crystal is described within crystal plasticity theory [7]. Crystal plasticity assumes that plastic deformation in single crystals takes place via simple shear on a specific set of planes. Deformation by other mechanisms such as, for example, diffusion, twinning and grain boundary sliding is not taken into the account in the present model. Details of the implemented crystal plasticity constitutive model are given, for example, in Ref. [8].

The combination of a slip plane, denoted by its normal m_i^α, and a slip direction s_i^α is called a slip system α. Type 316L stainless steel has a face-centered-cubic crystal structure and hence 12 slip systems denoted by $\{111\} < 110 >$. Symbols $\{l, m, n\}$ and $< l, m, n >$ denote respectively the family of (l, m, n) planes and family of $[l, m, n]$ directions that are identical due to the symmetry of the crystal.

The plastic velocity gradient $\dot{u}_{ij}^p$ due to a crystallographic slip can be written as [9]

$$\dot{u}_{ij}^p = \sum_\alpha \dot{\gamma}^\alpha s_i^\alpha m_j^\alpha \tag{2}$$

where the summation is performed over all active slip systems α, while $\dot{\gamma}^\alpha$ represents the shear rate. The cumulative slip γ over time t is defined as

$$\gamma = \sum_\alpha \int_0^t \left|\dot{\gamma}^\alpha\right| dt. \tag{3}$$

From the relation for small strain $\epsilon_{ij} = \frac{1}{2}(u_{ij} + u_{ji})$ one can obtain the plastic strain rate,

$$\dot{\epsilon}_{ij}^p = \sum_\alpha \frac{1}{2}\dot{\gamma}^\alpha \left(s_i^\alpha m_j^\alpha + s_j^\alpha m_i^\alpha\right). \tag{4}$$

The constitutive relation of the elasto-plastic crystal can be given in terms of stress and strain rates as [10]

$$\dot{\sigma}_{ij} = C_{ijkl}(\dot{\epsilon}_{kl} - \dot{\epsilon}_{kl}^p). \tag{5}$$

It is assumed that the shear rate $\dot{\gamma}^\alpha$ depends on the stress only via the Schmid resolved shear stress,

$$\tau^\alpha = s_i^\alpha \sigma_{ij} m_j^\alpha, \tag{6}$$

as

$$\dot{\gamma}^\alpha = \dot{a}^\alpha \frac{\tau^\alpha}{g^\alpha}\left|\frac{\tau^\alpha}{g^\alpha}\right|^{n-1}. \tag{7}$$

This is a reasonable approximation at room temperature and for ordinary strain rates and pressures [10]. Yielding is then assumed to take place when the Schmidt resolved shear stress exceeds the critical shear stress τ_0. In Eq. (7) $\dot{a}^\alpha$ represents the reference strain

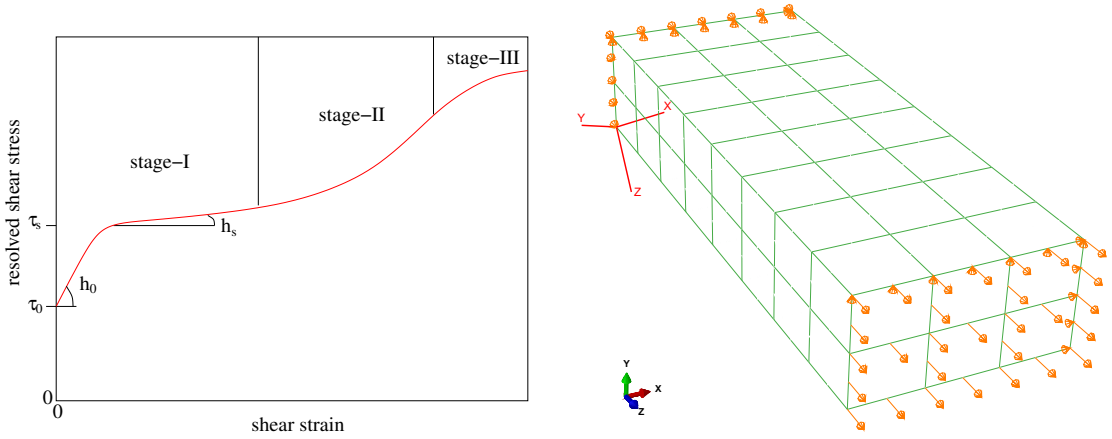

Figure 1: Left: definition of some of crystal plasticity material parameters in Bassani and Wu hardening model. Right: finite element model of the 316L stainless steel specimen gage section with dimensions $8.0 \times 3.0 \times 1.5$ mm. Arrows denote a tensile direction and boundary conditions. A local coordinate system assigns the initial material orientation (here [111] direction is chosen to be along the tensile direction).

rate, n the strain rate sensitivity parameter and g^α the current strain-hardened state of the crystal. In the limit $n \to \infty$, this power law approaches that of a rate independent material. The current strain-hardened state g^α can be derived from

$$\dot{g}^\alpha = \sum_\beta h_{\alpha\beta} \dot{\gamma}^\beta \tag{8}$$

where $h_{\alpha\beta}$ are the slip hardening moduli defined by the adopted hardening law. In this work the hardening law of Bassani and Wu is used [11].

The Bassani and Wu hardening law considers three stages of hardening of crystalline materials (see Fig. 1). The expression for self and latent hardening depends on the shear strains γ^α of all slip systems

$$\begin{aligned} h_{\alpha\alpha} &= \left\{ (h_0 - h_s)\mathrm{sech}^2 \left[\frac{(\mathrm{h_0} - \mathrm{h_s})\gamma^\alpha}{\tau_\mathrm{s} - \tau_0} \right] + \mathrm{h_s} \right\} G(\gamma^\beta; \beta \neq \alpha), \\ h_{\alpha\beta} &= q h_{\alpha\alpha}, \quad (\alpha \neq \beta) \end{aligned} \tag{9}$$

where h_0 stands for the initial hardening modulus, h_s for the hardening modulus during easy glide within the stage-I hardening, τ_0 for the yield stress, equal to the initial value of the current strength $g^\alpha(0)$, τ_s for the saturation stress or a reference stress where large plastic flow initiates [9], and γ for the total shear strain in all slip systems, Eq. (3). Parameter q is the latent to self hardening ratio, and

$$G(\gamma^\beta; \beta \neq \alpha) = 1 + \sum_{\beta \neq \alpha} f_{\alpha\beta} \tanh\left(\frac{\gamma^\beta}{\gamma_0} \right) \tag{10}$$

deals implicitly with cross-hardening that occurs between slip systems during stage II. Here, $f_{\alpha\beta}$ denotes the magnitude of the interaction strength between slip systems α and

β, while γ_0 represents the amount of slip after which the interaction between slip systems reaches the peak strength.

The above mentioned crystal plasticity theory along with the hardening law of Bassani and Wu [11] have been implemented numerically within the user subroutine UMAT written by Huang [9]. This UMAT subroutine has been used with finite element solver ABAQUS [12] for the present work. Note that UMAT allows to define one reference strain rate for one family of slip systems (hence $\dot{a}^\alpha \rightarrow \dot{a}$) and one value for the magnitude of the interaction strength between slip systems α and β (hence $f_{\alpha\beta} \rightarrow f_0$).

The crystal plasticity model has been implemented for finite deformations and rotations. The orientations of the slip systems are updated during every call to the UMAT and stresses are updated using the updated orientations.

2.2 Finite element model

Finite element simulations are performed by constructing a finite element model of the specimen gage section used in experimental studies [4] with second order reduced integration elements (C3D20R) available in ABAQUS [12], see Fig. 1. The number of elements used in simulations varies from 8 ($4 \times 2 \times 1$) to 2304 ($32 \times 12 \times 6$). A material orientation is assigned by introducing a local coordinate system into the ABAQUS model section. Initially, all the elements have the same material orientation. Note that for a given direction of straining ([001], [111] or [123]), a local coordinate system is defined up to an arbitrary rotation angle around the tensile axis (global Z axis). The effect of this angle is also briefly studied here.

Tension tests are simulated using displacement control analysis with the same strain rate as used in experiments (5×10^{-5} s^{-1}). Two simulation steps are used: in the first step the applied nominal strain is 0.003 (just above the yielding point) and in the second step the applied nominal strain is 0.5. Elastic deformation at the yielding point is estimated within the first simulation step at the point of maximum stress change. This value is then subtracted from the total strain to obtain the inelastic strain. The number of increments per simulation step is taken large enough to provide numerical stability and convergence: for [001] and [123] directions around 50 increments per step are enough, while for [111] direction at least 1000 of them are needed.

For boundary conditions, a constant displacement rate is specified in the axial direction (Z axis) for all the nodes on the front surface; the nodes on the back surface are constrained to have zero axial displacement. To avoid rotations around the tensile axis, additional constraints are prescribed to the following four edges: one vertical edge and one horizontal edge of the front surface (and similar on the back surface) are constrained in X and Y directions, respectively, as to remain straight and maintain a right corner during the deformation, see Fig. 1.

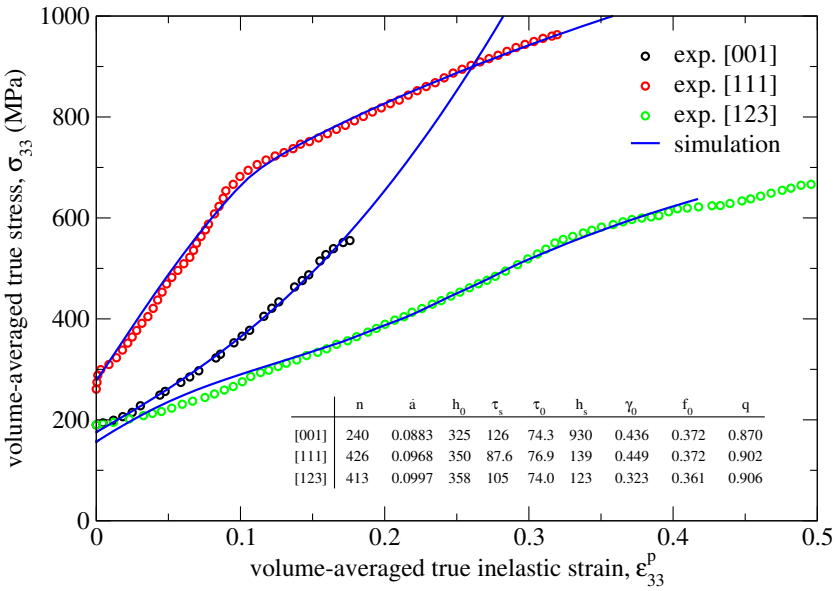

Figure 2: A comparison between experimental [4] (circles) and calculated (lines) tensile stress-strain curves obtained on a 48-element model. Each line was fitted separately to the corresponding experimental data; crystal plasticity material parameters for each orientation are also shown ($\dot{a}$ is in units of 1/s and h_0, h_s, τ_0, τ_s in MPa).

3 CALIBRATION PROCEDURE

In the calibration procedure the plastic material properties are changed so that the obtained numerical tensile curves of the three different crystal orientations (strained along [001], [111] and [123] directions) are fitted *simultaneously* to the corresponding measured true stress-strain curves of 316L stainless steel single crystals [4]. Identification of crystal plasticity material parameters is based on the assumption that all 12 slip systems, all belonging to one family, posses the same stress-strain behaviour (Fig. 1).

In the Bassani and Wu hardening model there are 9 material parameters involved: n, $\dot{a}$, h_0, h_s, τ_0, τ_s, γ_0, f_0, q. In principle, parameters h_0, h_s, τ_0, τ_s could be identified directly from the resolved shear stress versus shear strain curves, see Fig. 1. As our data is not available in such a form, all 9 parameters are instead found with our automatised optimization code.

In the optimization procedure, the optimal values for 9 material parameters are obtained by minimizing the χ^2 of the least-square fitting procedure to all three data curves,

$$\chi^2 = \left(\chi^2_{[001]} + \chi^2_{[111]} + \chi^2_{[123]}\right)/3 = \sum_{[...]} \sum_{i=1}^{m} \left(\sigma_i - \sigma_{33}(\epsilon_i^p, P)\right)^2 / 3(m-10) \qquad (11)$$

where σ_i and ϵ_i^p are respectively the measured true stress and true inelastic strain for a given crystal orientation ([...] in Eq. (11) stands for [001], [111] and [123]). The $\sigma_{33}(\epsilon_i^p, P)$ is the calculated volume-averaged true stress component along tensile direction (Z axis)

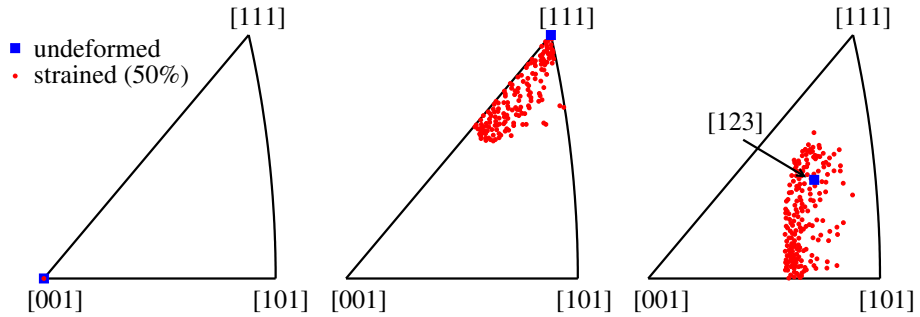

Figure 3: Calculated inverse pole figures showing the evolution of tensile axis orientations from undeformed to 50% strained state. Points represent orientations at the integration points of the finite element model. Material parameters used are the same as in Fig. 2.

obtained for a given crystal orientation and material parameter set P. The value of stress σ_{33} at the measured strain point ϵ_i^p is calculated from the interpolation of stresses at neighboring simulation strain points.

Minimization of χ^2 with respect to 9 crystal plasticity material parameters is performed using Powell's method [13]. Several runs with different initial parameter sets are tried in order to find the global minimum of χ^2. A two-way communication between ABAQUS and the minimization code is established through a separate fortran subroutine which enables an automatic identification of the parameters.

4 RESULTS

4.1 Calibration against individual data sets

Figures 2 and 3 present the results of simulations run with three different parameter sets calibrated separately against each of the three tensile data. In Eq. (11) this corresponds to minimizing separately $\chi^2_{[001]}$, $\chi^2_{[111]}$ and $\chi^2_{[123]}$. As can be seen from Fig. 2, almost perfect fits exist for all three tensile directions. The corresponding crystal plasticity material parameters (also shown in Fig. 2) do not differ considerably (except h_s) from one orientation to the other. This is encouraging in a sense that a reasonably good fit could also be found using only one common set of crystal plasticity material parameters.

Figure 3 shows the simulation results for the evolution of tensile axis orientations from undeformed to 50% strained state. The results predict a development of material orientation gradient for [111] and [123] loading directions. Unfortunately, no experimental analogue has been found in literature to validate the simulations.

4.2 Calibration against all data sets

Results of the calibration procedure, where the fits are performed to all three data sets simultaneously, are shown in Figs. 4 and 5. As anticipated, a very good agreement between the calculated lines and measurements in Fig. 4 can be found for all strains [15]. This confirms that a slip-based crystal plasticity model with Bassani and Wu hardening

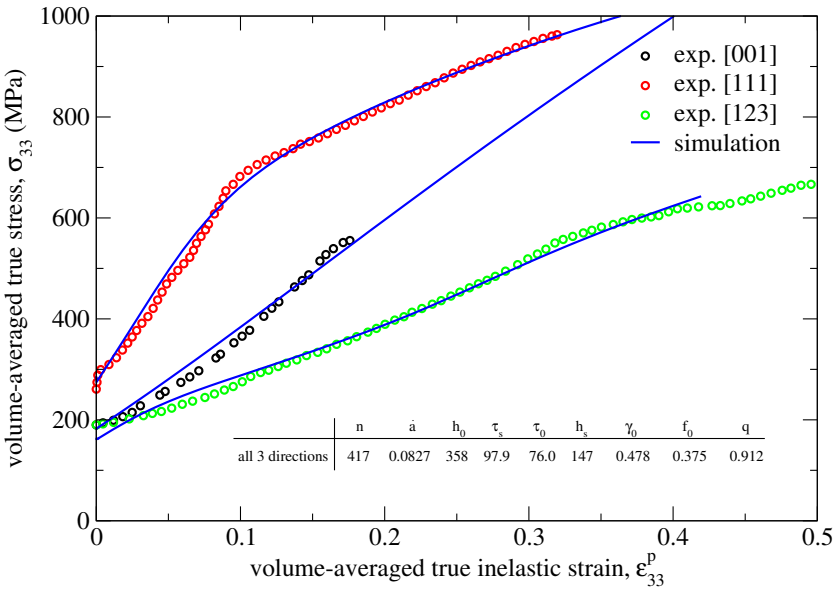

Figure 4: A comparison between experimental [4] (circles) and calculated (lines) tensile stress-strain curves obtained on a finest mesh with 2304 elements. All three lines were fitted simultaneously to the experimental data; the corresponding crystal plasticity material parameters are also shown ($\dot{a}$ is in units of 1/s and h_0, h_s, τ_0, τ_s in MPa).

can be used to describe tensile deformation behaviour of 316L stainless steel single crystals. In addition, the same results suggest that the combined effects of slip and twinning, which is also an important deformation mechanism in this type of steel [4, 5], can be modeled by slip alone (at least when considering stress-strain response).

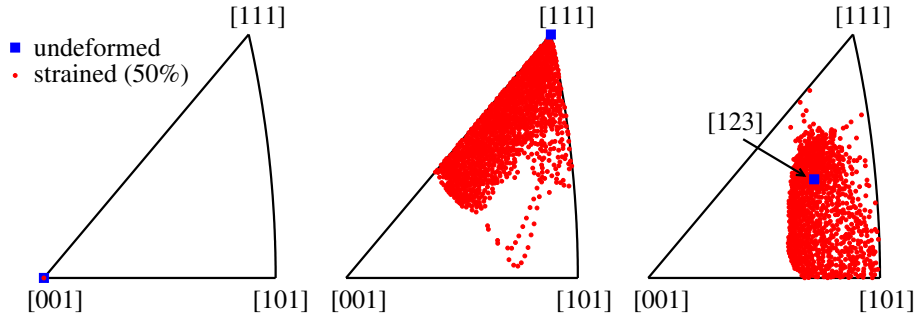

Figure 5: Calculated inverse pole figures showing the evolution of tensile axis orientations from undeformed to 50% strained state. Points represent orientations at the integration points of the finite element model. Material parameters used are the same as in Fig. 4.

Regarding texture evolution, however, the predictions of simulations shown in Fig. 5 still need to be validated against measurements. In particular, a development of quite large orientation gradients observed for [111] and [123] loading directions should be examined and compared in more detail.

4.2.1 Sensitivity analysis

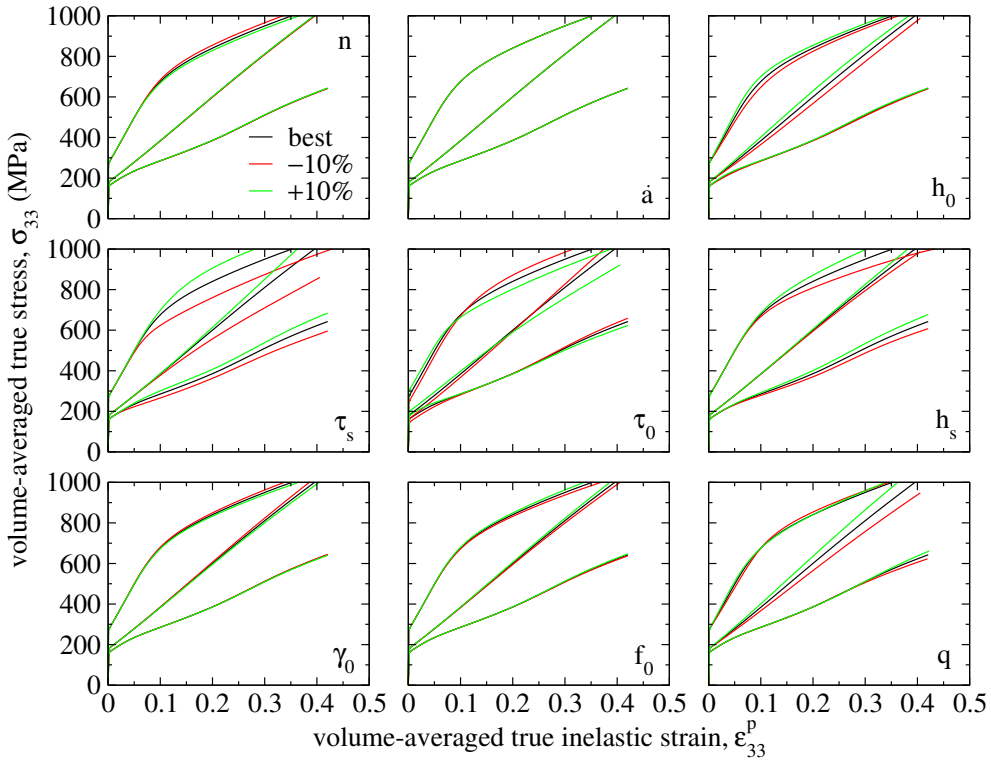

Figure 6: Sensitivity of the simulation results to a ±10% parameter change from its optimal value. One parameter is varied in each plot with the remaining parameters being fixed at their optimal values (see the table in Fig. 7). Results are obtained in a model with 288 elements.

A brief sensitivity analysis of the calibrating parameters is presented in Fig. 6. The largest influence on all three directions of straining have parameters τ_s and h_s. Slightly smaller influence, but mostly in [001] and [111] directions, have h_0 and τ_0, as well as q in [001] direction. These 5 parameters are therefore relatively well determined from the fits. On contrary, parameters $\dot{a}$, n, γ_0 and f_0 have higher ambiguity.

The influence of mesh density on the calibration output is checked by comparing best fit parameters on models with up to 2304 elements (Fig. 4). The quality of the fits is not reduced on smaller systems, however, a slight change is observed in the calibrating values. For example, comparing the parameter values in Fig. 4 with those obtained in a 288-element model (Fig. 7), the largest difference of 20% is observed for $\dot{a}$, while other parameters differ less than 4%. This again implies that $\dot{a}$ possesses biggest uncertainty.

Robustness of the calculated stress-strain curves is finally checked against different possibilities in selecting a material orientation (a local coordinate system in ABAQUS). As already discussed, for a given direction of straining ([001], [111] or [123]), a local coordinate system is defined up to an arbitrary rotation angle around the tensile axis. Since our

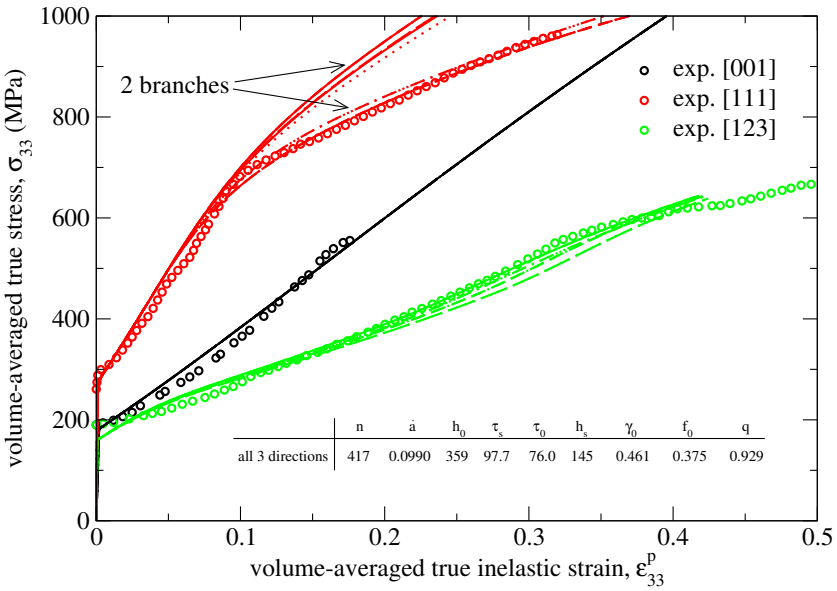

Figure 7: Calculated stress-strain curves as a function of material orientation uncertainty. Eight equidistant rotations from 0 to 2π (denoted by different line types) of material coordinate system around the straining (Z) axis are considered. Calibrating parameters are shown for the lower branch of the [111] response. In the model 288 elements are used.

model geometry is far from cylindrical, in principle the results should be affected by the choice of this angle. This is indeed observed in Fig. 7. While [001] and [123] directions show negligible dependence, the response in [111] direction is non trivial: seemingly two branches of solutions develop after reaching 10% of deformation. Note that in performing material calibrations always the lower branch is selected.

5 CONCLUSIONS

In this paper a procedure for automatic calibration of crystal-plasticity material parameters has been introduced and implemented in a slip-based crystal plasticity finite element model for single-crystal tensile measurements of type 316L stainless steel. Using the hardening law of Bassani and Wu, the calibrated parameters correctly predict the stress-strain response in all investigated directions. This suggests that the combined effects of slip and twinning, which is also an important deformation mechanism in this type of steel, can be effectively modeled by slip alone. The uncertainties of the calibrating parameters have been estimated for various mesh densities in a systematic single-parameter influence study on the calculated tensile curves.

ACKNOWLEDGMENT

The authors gratefully acknowledge the financial support from the Slovenian research agency through research program P2-0026.

REFERENCES

[1] Roters, F., Eisenlohr, P., Hantcherli, L., Tjanhjanto, D. D., Bieler, T. R., Raabe, D., 2010. "Overview of constitutive laws, kinematics, homogenization and multiscale methods in crystal plasticity finite-element modeling: Theory, experiments, applications". Acta Materialia 58, 1152-1211.

[2] Simonovski, I., Nilsson, K. F., Cizelj, L., 2005. "Material properties calibration for 316L steel using polycrystalline model". Proc. 13th Int. Conf. Nuclear Engineering, Beijing, China, 1-8.

[3] Gonzalez, D., Kelleher, J. F., Quinta da Fonseca, J., Withers, P. J., 2012. "Macro and intergranular stress responses of austenitic stainless steel to 90° strain path changes". Materials Science and Engineering A 546, 263-271.

[4] Karaman, I, Sehitoglu, H., Maier, H. J. and Chumlyakov, Y. I., 2001. "Competing mechanisms and modeling of deformation in austenitic stainless steel single crystals with and without nitrogen". Acta Materialia 49, 3919-3933.

[5] Karaman, I, Sehitoglu, H., Chumlyakov, Y. I. and Maier, H. J., 2002. "The deformation of low-stacking-fault-energy austenitic steels". JOM 54, 31-37.

[6] Simonovski, I., Cizelj, L., 2011. "Towards modeling intergranular stress corrosion cracks on grain size scales". Nucl. Eng. Des., 246, 107-114.

[7] Hill, R., Rice, J. R., 1972. "Constitutive analysis of elastic-plastic crystals at arbitrary strain". Journal of the Mechanics and Physics of Solids 20 (6), 401-413.

[8] Kovač, M., 2004. "Influence of microstructure on development of large deformations in reactor pressure vessel steel", PhD Thesis, University of Ljubljana.

[9] Huang, Y., 1991. "A User-Material Subroutine Incorporating Single Crystal Plasticity in the ABAQUS Finite Element Program". Tech. Rep. Division of Applied Sciences, Harvard University.

[10] Needleman, A., 2000. "Computational mechanics at the mesoscale". Acta Materialia, 48, 105-124.

[11] Bassani, J., Wu, T. Y., 1991. "Latent hardening in single crystals. II. Analytical characterization and predictions". Proceedings: Mathematical and Physical Sciences 435 (1893), 21-41.

[12] Simulia, 2012. ABAQUS 6.12-2.

[13] Press, W. H., Teukolsky, S. A., Vetterling, W. T., Flannery, B. P., 2007. "Numerical Recipes: The Art of Scientific Computing (3rd ed.)". New York: Cambridge University Press.

[14] Peirce, D., Asaro, R. J., Needleman, A., 1983. "Material rate dependence and localized deformation in crystalline solids". Acta Metall. 30, 1951-1976.

[15] Note that agreement is reduced considerably if Bassani and Wu hardening model is replaced by a simpler hardening model of Peirce, Asaro and Needleman [14].